Arabian Journal of Chemistry (2020) 13, 5724–5739

King Saud University

Arabian Journal of Chemistry

www.ksu.edu.sa
www.sciencedirect.com

ORIGINAL ARTICLE

NiO nanoparticle doped-PVA-MF polymer nanocomposites: Preparation, Congo red dye adsorption and antibacterial activity

Shahnawaz Ahmad Bhat [a], Fahmina Zafar [a,*], Azar Ullah Mirza [a], Aftab Hossain Mondal [b], Abdul Kareem [a], Qazi Mohd. Rizwanul Haq [b,*], Nahid Nishat [a,*]

[a] *Inorganic Materials Research Laboratory, Department of Chemistry, Jamia Millia Islamia, New Delhi 110025, India*
[b] *Departments of Bioscience, Jamia Millia Islamia, New Delhi 110025, India*

Received 31 December 2019; accepted 9 April 2020
Available online 18 April 2020

KEYWORDS

Polymer nanocomposite;
Antibacterial activity;
Adsorption

Abstract The standard of living has been improved by industrial "revolution" and the demand of new production increases due to population explosion. In the race of industrialization humans are busy discharging harmful gases in atmosphere, dumping unhealthy wastes in soil and discharging of toxic sewage in natural water resources. The present work reports the synthesis of polymer nanocomposite of blend encapsulated with NiO nanoparticles (K1-K5). The polymer nanocomposite films (K1-K5) were characterized by FTIR, XRD, TGA and SEM. The electrostatic interaction between the polymer matrix and encapsulated NiO nanoparticles increases the chemical stability in this order water > NaOH > HCl solution confirmed by contact angle (55° to 99°). The Congo red (CR) dye adsorption values increases in polymer nanocomposite films (K1-K5) were analyzed by an effect by an effect of contact time 45% to 68%, by an effect of CR dye concentration 48% to 70%. But the CR dye adsorption by S3 composite and nanocomposite films (K1-K5) are inversely proportional to the pH scale 4–10. Among four different bacterial strains *Bacillus subtilis* 25 mm and *Staphylococcus aureus* 25 mm has shown best antibacterial activity. The result confirms enhancement of antibacterial activity of S3 blend after the doping of NiO nanoparticles. The present results may be a roadmap to develop some transparent and flexible polymer nanocomposite films for water treatment in textile industries and efficient antibacterial activity.

* Corresponding authors.
E-mail addresses: fahmzafar@gmail.com (F. Zafar), nishat_nchem08@yahoo.com (N. Nishat).
Peer review under responsibility of King Saud University.

Production and hosting by Elsevier

https://doi.org/10.1016/j.arabjc.2020.04.011
1878-5352 © 2020 Published by Elsevier B.V. on behalf of King Saud University.

1. Introduction

The standard of living has been improved by industrial revolution and the demand of new production increase due to population explosion. Industrialization plays major role in discharging harmful gases in atmosphere and discharging of toxic sewage in natural water recourses. Synthetic dyes have been widely used in textiles, leather, plastic and printing. Congo red (CR) dye contains aromatic rings in their structure responsible for the carcinogenesis and bio-accumulation. It is also non-biodegradable, mutagenic and toxic for humans as well as aquatic systems (Ahmad and Kumar, 2010; Ayad and El-Nasr, 2010). Environmental legislation compels the industries to degrade or remove harmful dyes before releasing contaminated industrial water into the natural ecosystem. The decolorization of the dyes from wastewater is the main focus of consideration. Removing of a dyes is commonly treated by conventional techniques like coagulation, advanced chemical oxidation, (Zhou et al., 2018), photocatalysis, nano filtration, sedimentation (Joo et al., 2009) and adsorption (Vaghela et al., 2005). In recent years, encapsulation of metal oxide nanoparticles in the polymeric matrix and hybrid polymers have gained the attention of scientists because of their diversified applications (Meftah et al., 2014). Polyvinyl alcohol (PVA) is a green material due to its biodegradability, biocompatibility (DeMerlis and Schoneker, 2003), nontoxicity (Gopishetty et al., 2012) and illustrates swelling in water. However, some limitations associated with PVA instability in water is due to plasticizing action of water (Guzman-Puyol et al., 2015).

Dye adsorption technique is very simple and cheap, and has been used to extract azo dyes and heavy metals from aqueous solution by PVA/chitosan composites (Sekhavat Pour and Ghaemy, 2015). Composite films developed by the blending of PVA with different biodegradable and non-biodegradable polymers improve dye adsorption (Likozar et al., 2012). The stability of PVA in water has been improved by addition of Melamine formaldehyde (MF). MF resin usually increases stability and compatibility in PVA, but decreases transparency of PVA as the MF concentration increases (Yu et al., 2014). The thermal stability and resistance against hydrolysis enhanced by addition of MF resin in PVA (Xu et al., 2014; Kandelbauer et al., 2009).

The cationic azo dyes have been removed by magnetic nanocomposites based on starch-g-PVA functionalized with sulfate groups (Pourjavadi et al., 2016). Polymer nanocomposite derived from carboxymethyl tamarind-g-poly (acrylamide)/SiO_2 nanoparticles used as methylene blue dye adsorbent (Pal et al., 2012). PVA/magnetic kappa-carrageenan nanocomposite hydrogels used as adsorption beads to the removal cationic dyes (Mahdavinia et al., 2014). Novel Fe_3O_4/Thiacalix [4] arene tetrasulfonate self-doped/polyaniline/nanocomposite used for cationic dye adsorption (Lakouraj et al., 2015). Sodium alginate/organic polymer nanocomposite has been used for absorption of methylene blue (Thakur et al., 2016).

Pathogenic bacterial infection is a global problem becoming a dominant obstacle in scientific research in the present century. Therefore, there is need for an hour to design and develop new class of polymer nanocomposites used for the treatment of dye contaminated water and act against pathogenic microbes. PVA composite with kappa-carrageenan to prepare composite used for biomedical and drug delivery applications (Wu et al., 2016) and PVA/poly methyl methacrylate composite used for healing chronic wounds (Hsieh et al., 2017). Enhancement of the antibacterial activity by PVA was observed after blended with quaternized cellulose (Hu and Wang, 2016) and with MF (Bhat et al., 2020). The metal/metal oxide nanoparticles have shown the biological applications, due to quantum size effects, fast diffusivities, large surface area than the bulk materials (Ichiyanagi et al., 2003; Karthik et al., 2011; Gandhi et al., 2010). Among the various metal oxide nanoparticles, NiO nanoparticles are very important nanomaterials extensity were used as catalyst and antibacterial agents (Ajoudanian and Nezamzadeh-Ejhieh, 2015; Helan et al., 2016). Nanocomposite developed from PVA/chitosan/silver has shown antibacterial activity against different microbes (Elbarbary and El-Sawy, 2017; Ayeshamariam et al., 2015). Electron spun based nanocomposite was used for wound dressing applications (Hassiba et al., 2017). The potential biomedical applications have been shown by iron-oxide nanoparticle/PVA Ferro gels nanocomposites (Mendoza Zélis et al., 2013). Silver based nanocomposite has shown various applications like optical, electronic devices and antimicrobial agents (Matsuda et al., 2005). ZnO nanoparticles embedded in PVA/chitosan composites are also used in biomedical applications (Azizi et al., 2014).

Literature search reveals that MF affects the properties of PVA such as thermal stability, moisture resistance, surface smoothness, resistance in abrasion, hardness and flame retardant which gained attention of industrialists (Wang, 2015). Therefore it would be of interest evaluating the effect of NiO nanoparticles in (PVA-MF) S3 composite (Bhat et al., 2020). The present work is purposeful to improve water instability and best of knowledge, to investigate for first time physical properties, swelling properties, contact angle and antibacterial activity of PVA-MF/NiO polymer nanocomposite films. The polymer nanocomposite films were characterized by FT-IR for the determination of chemical interaction and functional groups. XRD was used to determine crystalline and amorphous nature of materials, contact angle for hydrophobicity and SEM technique for surface morphology of films. The objective of the work is (i) determination of swelling studies and biodegradation of nanocomposite films, (ii) evolution of polymer nanocomposite as an adsorbent for CR dye adsorption from water, assessment of experimental conditions such as an effect of contact time, effect of the pH solution, and an effect of CR dye concentration. (iii) the investigation of antibacterial activity against Gram-positive *Bacillus subtilis (B. subtilis)* 4736 and *staphylococcus aureus (S. aureus*) 5902, and Gram-negative *Escherichia. coli (E. coli)* 25922, *Klebsiella pneumoniae (K. pneumoniae)* 700603 bacterial strains.

2. Materials and methods

$NiCl_2{\cdot}6H_2O$ and $NaHCO_3$, PVA M.W 85000–1 24,000 (L.R grade) and formaldehyde (37% w/v, R L) were bought from Merck India. Melamine (AR grade), double distilled water and NaOH were purchased from Gujarat Natural Fertilizers Limited India. CR dye and Mueller-Hinton agar, well plates and patri plates were purchased from JKM LABTEK laboratories, New Delhi India. The Gram-positive bacterial strains *Bacillus subtilis* MTCC 736, *Staphylococcus aureus* MTCC 902 was obtained from CSIR Institute of Microbial

Technology, Chandigarh, India and Gram-negative *Escherichia coli* ATCC 25922 and *Klebsiella pneumoniae* ATCC 700603 from Microbiology Research Laboratory, Jamia Millia Islamia, New Delhi, India.

2.1. Synthesis of NiO nanoparticles

NiO nanoparticles were synthesized by co-precipitation method by following procedure (Bhat et al., 2019).

2.2. Synthesis of Melamine-formaldehyde

The Melamine-formaldehyde resin (1:3) ratio was prepared with some modification in the well-known method (Merline et al., 2013). The synthesis of MF resin occurs in two stages. Methylolation is first addition reaction of formaldehyde and melamine formaldehyde that can be carried out in a basic medium. The condensation reaction is second stage leading to the development of ether linkage that can occur due to crosslinking in alkaline condition. The formation of MF resin was confirmed by FT-IR.

2.3. Synthesis of PVA-MF composites

The PVA-MF composite was prepared as mentioned in the reported work (Bhat et al., 2020). To prepare PVA stock solution 10% PVA was added to double distilled water and the solution was heated on a magnetic stirrer at 90 °C for 2 h. The freshly prepared MF resin and prepared 20 mL of PVA solutions were blended with some modifications in various ratios (Merline et al., 2013) (MF 13%, 23%, 33% and 43%) by using a magnetic stirrer. Condensation reaction between PVA with different MF ratios (PVA-MF composites) at 90 °C was carried out until the white colour appears in the reaction mixtures as shown in step III. The formation of composite was confirmed by FT-IR. The prepared PVA-MF composite with 77:23 ratio (S3) was selected for the preparation of polymer nanocomposite.

2.4. Synthesis of polymer nanocomposites

Stock solution of 10% PVA was synthesized by dissolving in double distilled water and the solution was heated on the magnetic stirrer at 90 °C for two hours. The freshly prepared MF and the prepared 20 mL of PVA solution was reacted with some modification in various ratios (Bhat et al., 2019). The S3 composite solution was heated on a magnetic stirrer at 90 °C up to one hour and the white colour appearance confirms the synthesis of S3 composite shown in Fig. 1. The synthesized NiO nanoparticles then sonicated in double distilled water for 30 min. Polymer nanocomposite was synthesized by ex-situ method (Bhat et al., 2019) by the dispersion of different percent of NiO nanoparticles labeled as K1 (1%), K2 (2%), K3 (3%), K4 (4%) and K5 (5%) in 77:23 S3 composite respectively shown in Fig. 2.

2.5. Preparation of polymer nanocomposite films

The smooth and air bubble free thin uniform films obtained by pouring desired amount of polymer nanocomposite (K1-K5) solutions on rectangular Teflon sheet. The samples were put uninterrupted till dried at moderate temperature (28–35 °C) for 12 h after drying the films then the samples were packed in zip lock bags.

3. Characterizations

The chemical crosslinking and electrostatic interaction among functional groups of S3 composite and NiO nanoparticles in polymer nanocomposites were analyzed by various analytical and instrumental measurements.

Fourier transform infrared (FT-IR) spectra of S3 composite and polymer nanocomposite films (K1-K5) in the range of 600–3500 cm^{-1} region were taken on a PerkinElmer 1750 USA. UV visible DRS spectra and absorption studies were carried out by Shimadzu UV 2550 Japan. UV visible spectrophotometer ranges from 200 to 800 nm.

X-ray diffraction (XRD) studies have been carried out using Rigaku Ultima IV X-ray diffract meter with Ni-filtered Cu-Kα radiation Japan (λ = 1.5416 Å).

Morphology and structural analysis of S3 composite and polymer nanocomposite films (K1-K5) were analyzed by Scanning electron microscope (SEM model FEI Quanta 200 FIE 250 X Max 80 USA) at SAIF research laboratory All India Institute of medical science, New Delhi India.

Thermo gravimetric analysis (TGA) of S3 composite and polymer nanocomposites films (K1-K5) were studied by Metter Toledo AG analytical CH860, Schwerzenbach, Switzerland) at NIT Srinagar performed in a range of 250–850 °C at a heating rate of 10 °C/m under nitrogen gas 20 mL/min.

The contact angle of water on the polymer nanocomposite films (K1-K5) were determined with a drop system analysis (KRUSS BmbH Co., Germany) based on the sessile drop method in a room temperature and 60% relative humidity. Average contacts of all samples were taken from at least two different points on the film surface.

3.1. Swelling studies

The swelling and chemical stability of polymer nanocomposite films (K1-K5) were carried out in three parameters such as 0.1 M solution of HCl, NaOH and double distilled water at 25 °C at different time intervals and the swelling percentage was calculated by equation (1).

$$\text{Swelling}\% = \frac{S_w - S_D}{S_D} \times 100 \quad (1)$$

S_w is the weight of a wet sample and S_D is the weight of a dry sample.

3.2. Soil degradation test

Soil degradation test was determined in natural environment. The weight and size of pure polymer nanocomposite films are 0.013 g and 1.5 cm × 1.5 cm, buried 30 cm below the soil in Jamia Millia Islamia. The temperature of soil, pH and moisture of air was measured as 18.2 °C, 7.6 and 52% respectively. After 30 days all samples were taken out washed properly so that attached soil was washed away then dried at 40 °C for 4 h. After every weak the weight loss was calculated after the

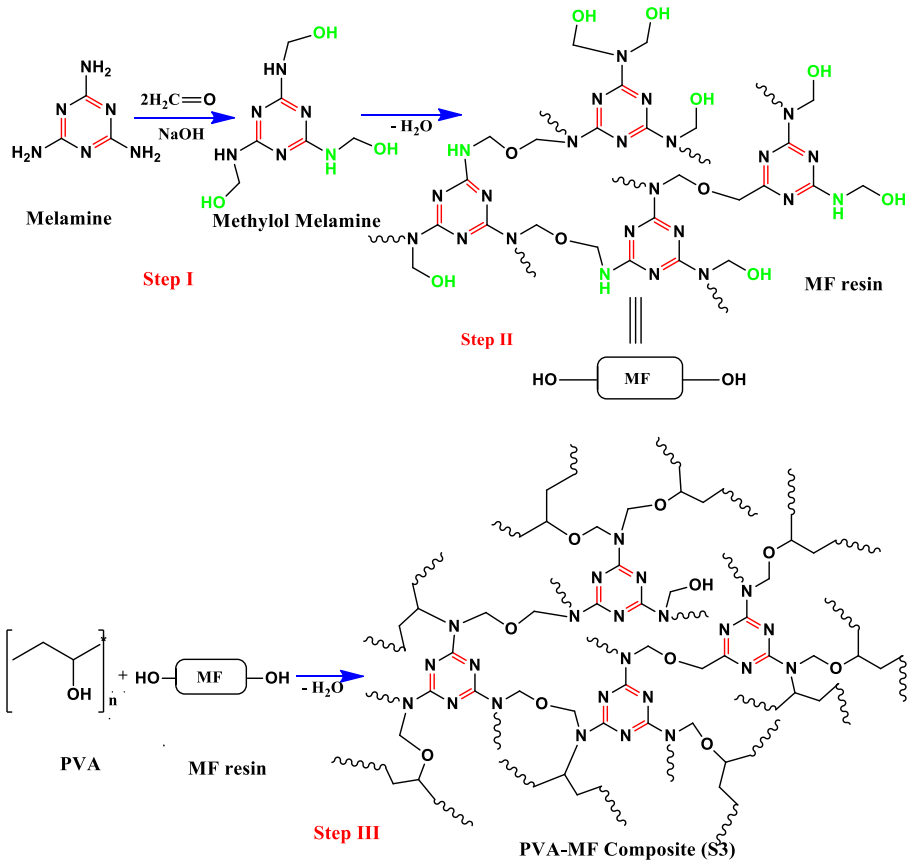

Fig. 1 Reaction scheme of polymer composite.

burial. The average weight loss was calculated by the following equation (2).

$$\text{Weight loss}\% = \frac{\text{Wi} - \text{Wf}}{\text{Wi}} \times 100 \quad (2)$$

W_i is initial weight and W_f is final weight of polymer nanocomposites.

3.3. Adsorption experiment by using batch method

The adsorptions of CR dye by S3 composite and polymer nanocomposite films (K1-K5) were determined by batch adsorption method. A standard solution of 500 mg/L CR dye was prepared by dissolving CR dye powder in double distilled water. The CR dye solution was watered to various concentrations 50–200 mg/L. Before adsorption S3 composite and polymer nanocomposite films (K1-K5) were dried in a vacuum desiccator. CR dye adsorption was carried in a series containing 10 mL (50 ppm) dye solution having 0.013 g adsorbent bead of polymer nanocomposite films (K1-K5), the concentration of CR dye (50, 100, 150 and 200 mg/L), the pH of solution (4, 6, 8, 9 and 10) and agitation time of solution (10–60 min) at 30 °C. The pH of the solution was adjusted by 0.1 M HCl and NaOH. In all three parameter solutions were shaken by thermostatic shaker at 250 rpm. The experiment was repeated in all three parameters for justification of results.

The percent removal of CR dye (mgL^{-1}) by polymer nanocomposite films (K1-K5) was calculated by using a mass balance relationship, which determines the quantity of CR dye adsorbed per unit weight of adsorbent by Eq. (3).

$$\text{Removal}\% = \frac{\text{Co} - \text{Ce}}{\text{Co}} \times 100 \quad (3)$$

where Co and Ce ($mg\ L^{-1}$) before and after CR dye adsorption.

3.4. Antibacterial activity

Antibacterial activity of polymer nanocomposite films was investigated against Gram-positive and Gram-negative bacterial strains. The antibacterial activity of nanocomposite was performed according to Kirby-Bauer disc diffusion method with slight modification (Bauer et al., 1966). Briefly, all the bacterial strains were separately streak on Luria agar media (Himedia, India) plates and incubated overnight at 37 °C. After incubation, pure single colony of each strain was inoculated into 10 mL sterile Luria broth (Himedia, India) and incubated at 37 °C in automated incubator shaker at 120 rpm for 5 h to obtained log phase bacterial culture. Further, the log phase culture was diluted in same media adjusted absorbance 0.1 at 600 nm to obtained 0.5 McFarland ($1–2 \times 10^8$ CFU/ml) as mentioned in Kirby-Bauer disc diffusion method. Finally, equal volume (50 µL) of bacterial culture spread on Mueller Hinton Agar (MHA, Himedia, India) plates and almost equal size of polymer nanocomposite films (K1-K5) were placed at appropriate distance on each plate. Antibiotic

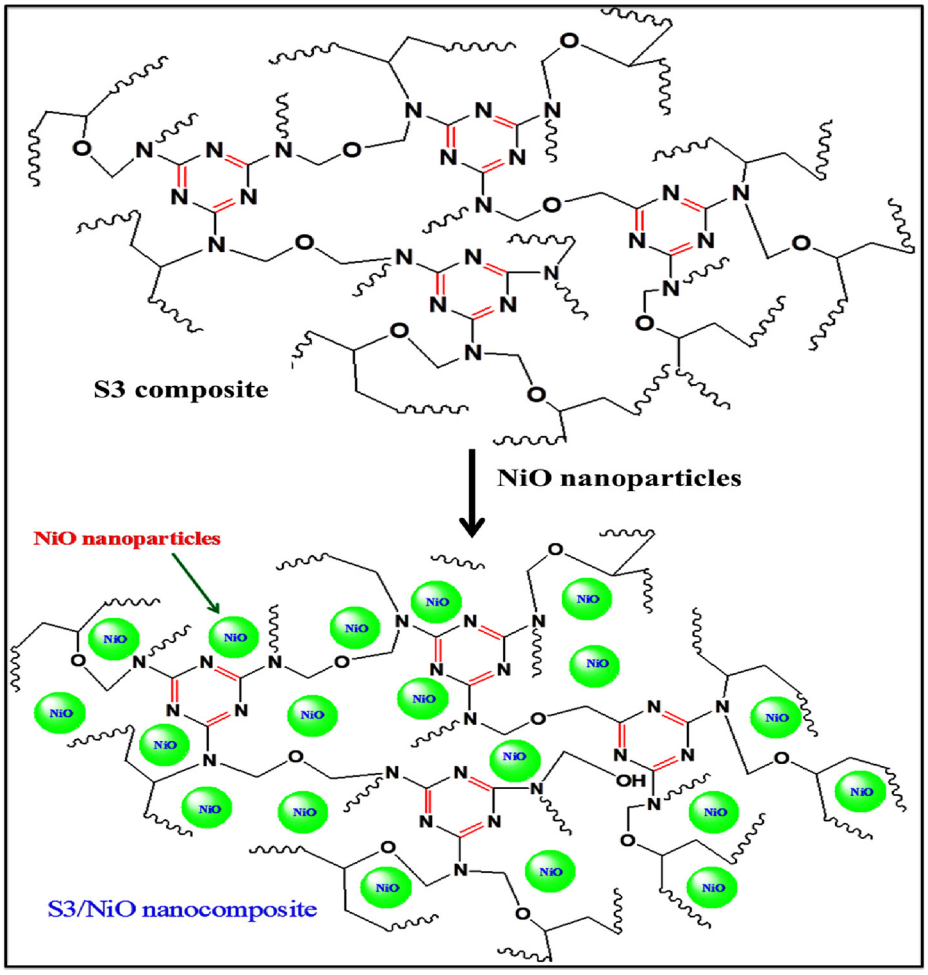

Fig. 2 Reaction scheme of polymer nanocomposites (PVA-MF/NiO) formation.

disc containing 10 μg of Cefotaximine (CTX) was used as a positive control in each plate. All the culture loaded MHA plates were incubated at 37 °C for overnight. After incubation the clear ZOI for test composite and cefotaxime (control) in each plate was measured at mm scale to determine the antibacterial efficacy.

4. Results and discussion

Synthesis and characterization of polymer nanocomposite are discussed below:

4.1. Spectral analysis

4.1.1. FT-IR

FT-IR spectra of polymer nanocomposite films (K1-K5) showed drift of peaks as well as some additional peaks in comparison to S3 composite shown in Fig. 3 (Bhat et al., 2020). The electrostatic interaction between S3 composite and NiO nanoparticles in polymer nanocomposite leads to the shifting broad peaks from S3 composite 3456 cm^{-1} to 3419–3380 cm^{-1} assigned to O-H stretching of (K1- K5) nanocomposite films (Guo et al., 2014). The C-H peak of S3 composite was shifted from 2960 cm^{-1} to 2939–2958 cm^{-1} in (K1-K5) due to electrostatic interaction respectively (Ahad et al., 2012). The C = N stretching peaks were observed at 1552–1556 cm^{-1} in nanocomposites and the C-H bending peak of CH_2 was shifted from S3 composite 1465 cm^{-1} to 1455–1456 cm^{-1} in all nanocomposites correspondingly (Bhargav et al., 2009). The visible peaks at 1339–1344 cm^{-1} referred to C-N stretching (Choma et al., 2012). The shifting of peak from S3 composite 1064 cm^{-1} to 1081–1087 cm^{-1} corresponds to C-O-C stretching confirms the chemical crosslinking between PVA and MF and electrostatic interaction within polymer nanocomposites (K1-K5) reported by Razavi (Yang et al., 2013). The strong peak shifts from 810 cm^{-1} to 813 cm^{-1} attributed to triazine ring of MF resin and the peak appeared broad and short in all polymer nanocomposites (K1-K5) (Razavi et al., 2011; Merline et al., 2013). The additional peak appears in all nanocomposites at 415 cm^{-1} to 466 cm^{-1} corresponds to Ni-O stretching vibration in all nanocomposites (Farzaneh and Haghshenas, 2012). After cross-linking with OH group of PVA, OH/NH groups of MF and electrostatic interaction with NiO nanoparticles shifts the peaks to higher wavenumber in all nanocomposites (K1-K5).

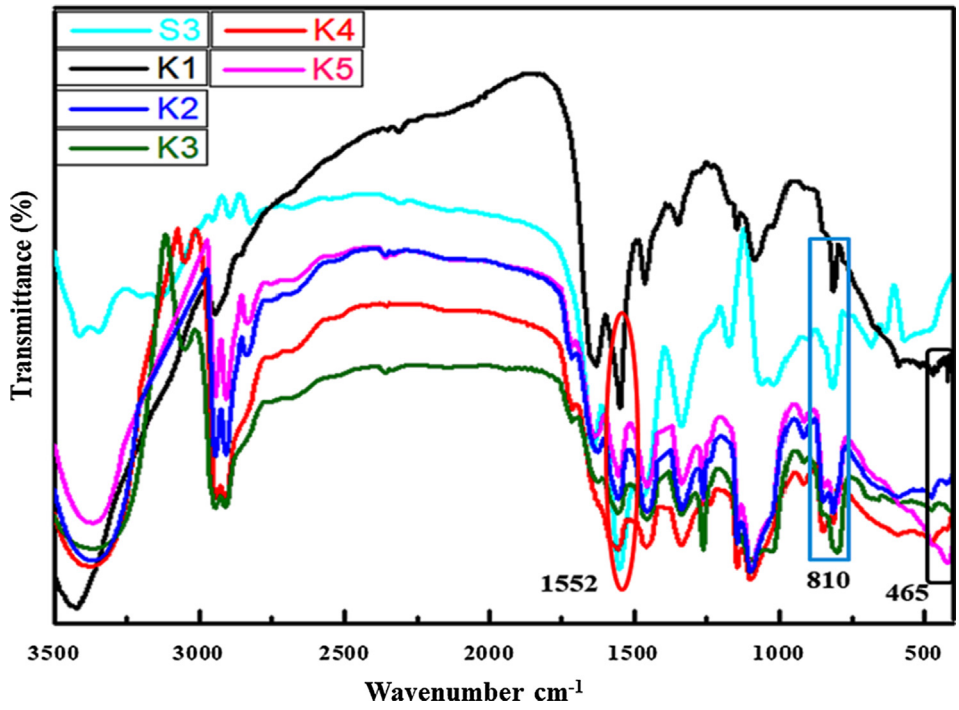

Fig. 3 FT-IR of polymer nanocomposites films of S3 (Bhat et al., 2020) and K1-K5.

4.2. UV visible DRS spectroscopy

UV–visible spectroscopy is one of the vital techniques to reveal the energy structures and a chemical shift in the polymer nanocomposite. Fig. 4 shows the UV–visible absorption spectra shift from S3 composite 239 nm to 324 nm after encapsulation of NiO nanoparticles in polymer nanocomposite. The strong absorbance peak of NiO nanoparticles in the UV region was observed at a wavelength of about 284 nm, 320 nm (Rudko et al., 2013). The chemical shift has been observed by encapsulation of metal/metal oxide nanoparticles in the PVA and glucose (El-Kemary et al., 2013). The reduction of band gap takes place from S3 composite (5.05 eV) to (4.36 eV) in nanocomposites in UV region. The decrease in band gap is associated with the electronic transition from filled valence band to the empty conduction band due to doping of NiO/CuO nanoparticles in PVA based nanocomposites (Udagawa et al., 2016). The small size of semiconducting nanoparticles in polymer nanocomposites approaches the radius of excited-state orbital of conduction band to examine the quantum size effect: the red shirt and blue shift has been observed in Cd/PVA polymer nanocomposite (Rudko et al., 2013). Dramatically red shift increase as the concentration of NiO nanoparticles increases in the S3 composite.

4.3. Morphology

4.3.1. XRD

XRD is used to analyze the phases, amorphous and crystalline nature of composite and polymer nanocomposite films. The 2θ value at 19.66° is a characteristic peak of amorphous S3 composite film. Fig. 5 shows that the new peaks appeared with 2θ value at 37.77° _ (1 1 1), 43.06_ (2 0 0) and 62.83_ (2 2 0) in the polymer nanocomposite films (K1-K5) and the peak intensities increases as the concentration of NiO nanoparticles in the S3 composite polymer matrix. The XRD of spectra shows three sharp peaks of NiO nanoparticles at 2θ 37.77° _ (1 1 1), 43.06_ (2 0 0) and 62.83_ (2 2 0) reported by Elbarbary (Udagawa et al., 2016) confirms the formation of polymer nanocomposite (K1-K5). The peak intensity at 19.66° of polymer nanocompostes also increase as the wt. % of NiO nanoparticles increases. As the peak intensity of polymer nanocomposite increases the amorphous nature decreases but enhances the semicrystalline nature of polymer nanocomposite films (Meftah et al., 2014).

4.4. SEM analysis

The appearance of new peaks in FT-IR and XRD of nanocomposite is semi crystalline state due to the doping of NiO nanoparticles in S3 composite confirmed by SEM micrograph. This technique is used to determine the morphology of S3 composite shows the smooth and uniform surface of S3 composite as shown in Fig. 6(a) (Bhat et al., 2020). The surface morphology and the uniform distribution of NiO nanoparticles in the polymer nanocomposite at (20 and 2 μm) magnification and the shape of encapsulated nanoparticles in the polymer nanocomposite are spherical as shown in Fig. 6(b and d). The nanoparticles are clearly visible in PVA/Ag nanocomposites shown in the SEM reported by Kashihara (Elbarbary and El-Sawy, 2017). To determine the narrow size and excellent distribution of nanoparticles the SEM images can be used to draw the histogram with the help of ImageJ software (Longo et al., 2011). The average size of NiO nanoparticles is 55 nm and the shape is spherical in polymer

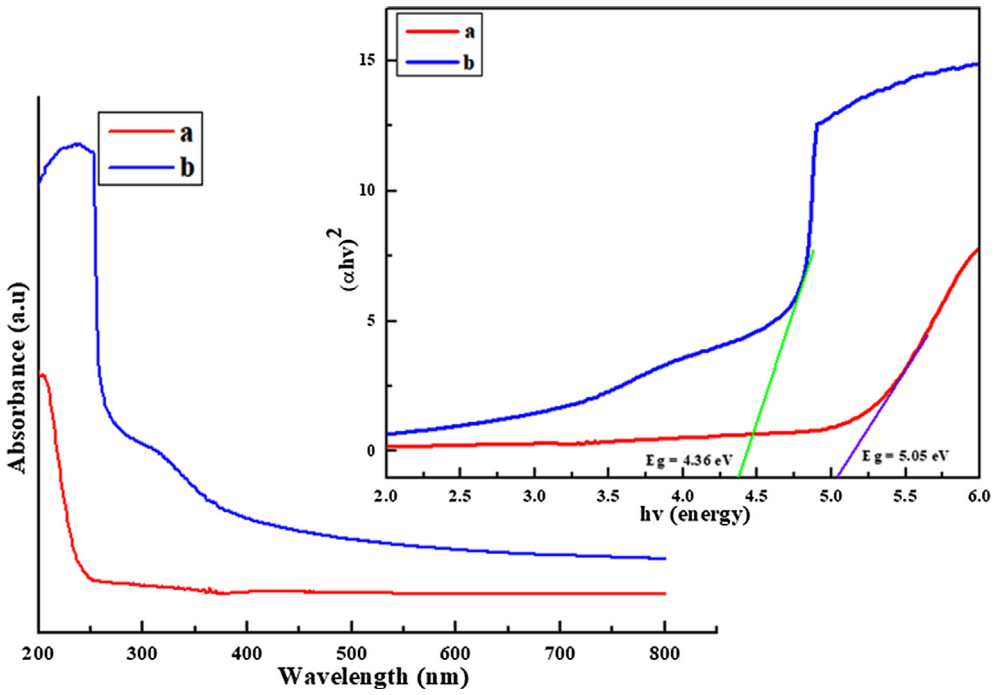

Fig. 4 UV–Vis spectra of pure (a) S3 composite and (b) polymer nanocomposite.

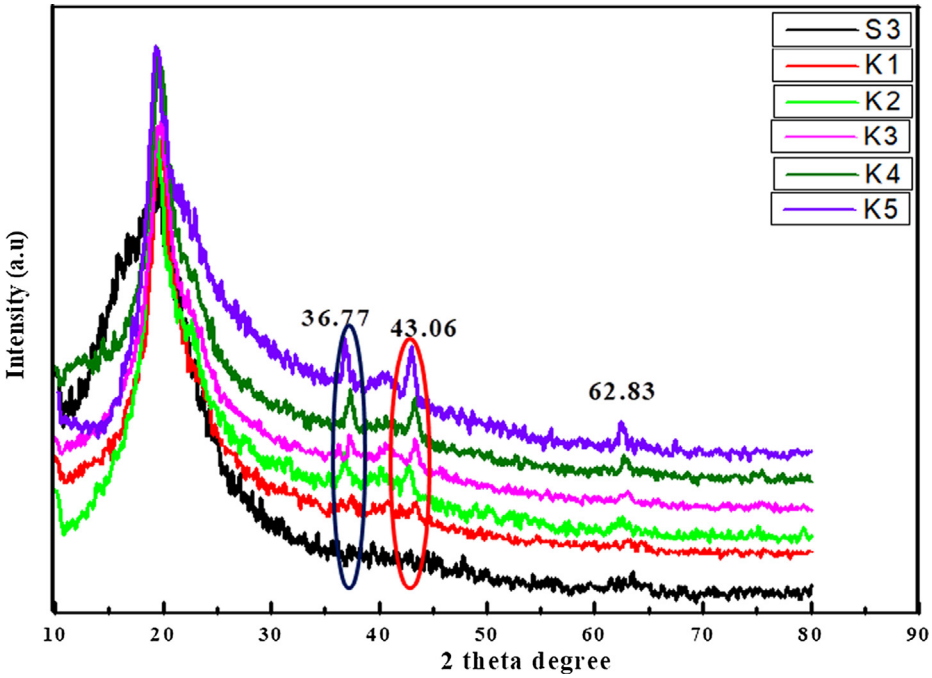

Fig. 5 XRD micrograph of polymer nanocomposites.

nanocomposites as shown in Fig. 6(d). The NiO nanoparticles increase the crystallinity in the polymer nanocomposite.

5. Contact angle

The significant changes on the surface morphology of polymer nanocomposites (K1-K5) observed in the SEM images has been confirmed by the measurement of contact angles as shown in Fig. 7 (Kashihara et al., 2018). The improvements in moisture resistance of polymer nanocomposite (K1-K5) films were analyzed by contact angle with a water drop method. Contact angle is the angle between nanocomposite film-water interactions at interfaces. It was observed that contact angle increases as NiO ratio was increased in S3 composite as shown in Fig. 7 (K1-K5). The contact angle increases from (55–91°) was observed on the polymer nanocomposite

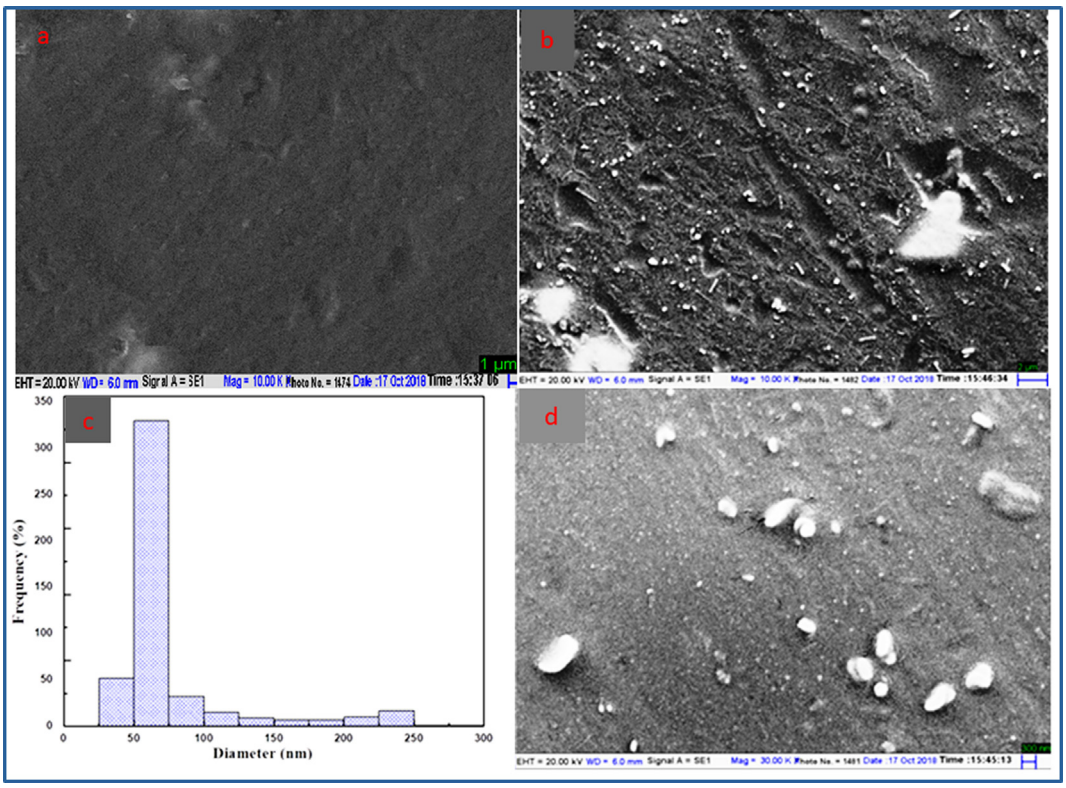

Fig. 6 SEM images of S3 composite (a), polymer nanocomposite (b and d) at 20 μm and 2 μm revealing surface morphology of polymer nanocomposite (c) histogram of polymer nanocomposite (K3).

(K1-K5) films after addition of 1–5% of NiO nanoparticles in S3 composite. The contact angle below 90° is hydrophilic materials and above 90° are hydrophobic materials. Polymer nanocomposites (K1-K5) with contact angle below 90° shows good wetting property and the contact angle above 90° shows poor wetting property. The result reveals that contact angle increases from 55 to 91° confirms the improvement in moisture resistance.

5.1. Swelling properties

The swelling behaviour of polymer nanocomposite films (K1-K5) were determined by placing the uniformed size and pre-weighted film samples in different conditions like distilled water, (0.1 M) solution of HCl and NaOH solution. The polymer nanocomposite films were weighted before and after the immersion in the different solutions at the specific time intervals to observe the swelling and chemical stability of nanomaterials. The film samples immersed in the distilled water and the maximum swelling percent attained by S3 composite films 771% and minimum swelling shown by nanocomposite films 620% which was attained due to maximum osmatic pressure. The swelling properties of polymer nanocomposite are very sensitive towards the ionic solutions. The swelling in 0.1 M HCl solution of S3 composite (44–77%) within 30 min then the composite film degrades, but the swelling decreases from (74–66%) in polymer nanocomposites confirm that the chemical stability increases in polymer nanocomposite as compared to S3. The maximum swelling of composite (469%) and the reduction of swelling from (451–351%) in polymer nanocomposite films (K1-K5) due to lowering of osmatic pressure in (0.1 M) NaOH basic solution as compared to water. The result reveals that the swelling properties of S3 composite and polymer nanocomposite films (K1-K5) were affected due the charge generated in three different parameters such as distilled water, (0.1 M) solution of HCl and (0.1 M) NaOH solution. The swelling behavior of S3 composite reduction capability increases from (K1-K5) due to chemical crosslinking between PVA and MF resin by consuming hydroxyl groups present in both reactants (Wei et al., 2015) and the electrostatic interaction between NiO nanoparticles (Satheesh Kumar, 2007; Anisha et al., 2013). The swelling percent decreases as the wt. % of NiO nanoparticles increases and chemical stability increase in the polymer nanocomposite. The stability in all three conditions increases after addition of NiO nanoparticles in S3 composite as shown in Fig. 8.

5.2. Biodegrability test

The biodegradation of pure S3 composite films occur due to enzymatic action of microorganisms present in soil (Gerlach et al., 2005; Ahmad et al., 2017). The degradation rate of S3 composite films were more than polymer nanocomposite films (K1-K5) after 30 days of soil burial. Fig. 9 shows the weight loss was low initially but increases with time reported in the above work. The bacteria responsible for bio-degradation of S3 composite film (S3) by *Rhodococcus opacus, Agrobacterium tumefaciens* and *Pseudomonas putida* mineralize atrazine ring to CO_2 and NH in the contaminated soil (Mandelbaum et al., 1995). The polymer nanocomposite samples showed lowest weight loss due to electrostatic interaction, uniform surface and hydrogen bonding with NiO nanoparticle within the

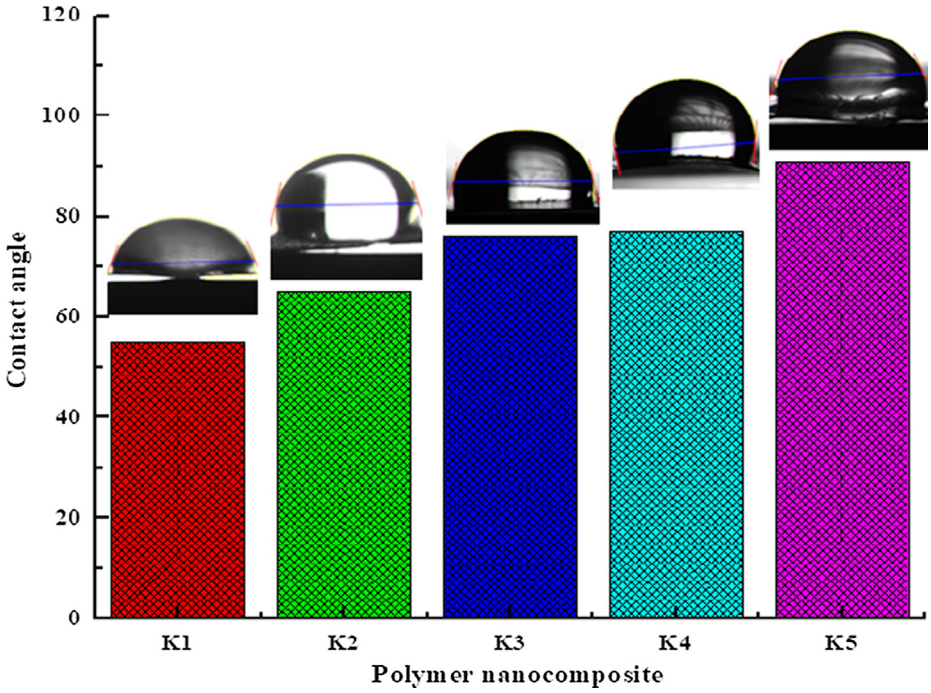

Fig. 7 Contact angle of polymer nanocomposite films.

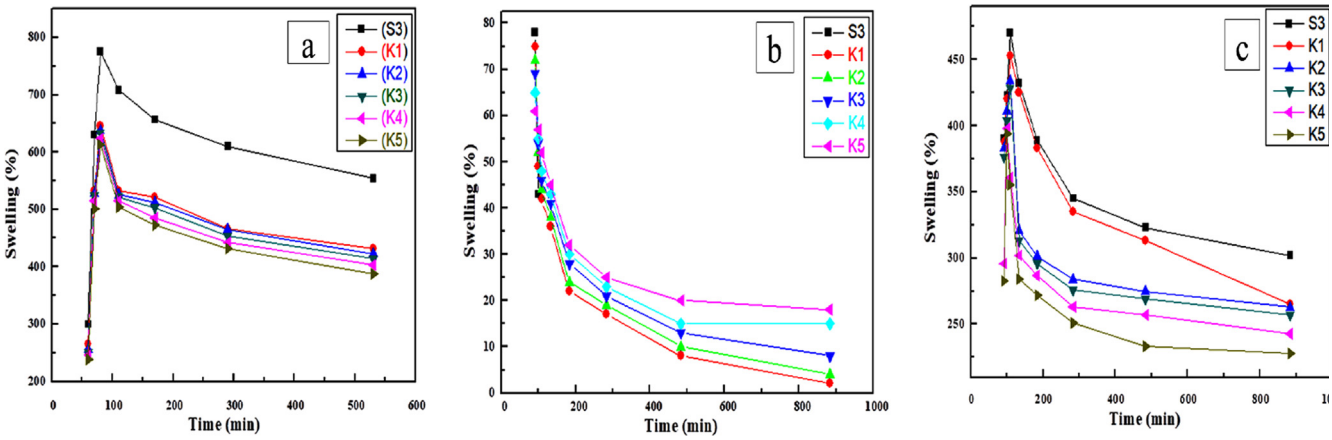

Fig. 8 Swelling ratios in (a) water (b) HCl (c) NaOH as function of time polymer nanocomposite at room temperature.

cross-linked network increases the compactness of the nanocomposite films. It was analyzed that after burying the polymer nanocomposite films (K1-K5) in the soil, the polymer nanocomposite films became hard. The soil degradation of sweet potato starch film increases after the addition of montmorillonite (MMT) nano clay and thyme essential oil (Issa et al., 2018). The available pores in the composite film filled with NiO nanoparticles decreases the probability of degradation. So the concentration of NiO nanoparticles affects the soil degradation of S3 composites.

5.3. Thermal analysis

5.3.1. TGA

Thermogravimetric analysis of PVA-MF composite has been reported by Bhat et al. (Merline et al., 2013)*. The TGA of polymer nanocomposites (K1-K5) shows three main weight loss stages (Fig. 10), the first stage starts from 80 to 220 °C (7–6 wt% loss due to vaporization of water and other moieties), second stage, starts from 220 to 410 °C (67–54 wt% loss due to side chain decomposition of PVA and ammonia from MF) and the third stage, starts from 410 to 500 °C (75–62 wt% due to decomposition of the main chain of PVA and MF produces volatile compounds like CO_2, HCN and CO) (Pirzada et al., 2012). By comparing the weight loss among S3 composite and polymer nanocomposite (K1-K5) films showed that thermal stability increases in polymer nanocomposites. The degradation of MF and the formation of volatile by products such as CO_2, HCN, and CO. The thermal stability of polymer nanocomposite films (K1-K5) increase due to the electrostatic interaction, network structure of NiO nanoparticles with un-reacted hydroxyl groups and small pores filled with nanoparticles leads to hydrogen bonding and the molecular chain rigidity.

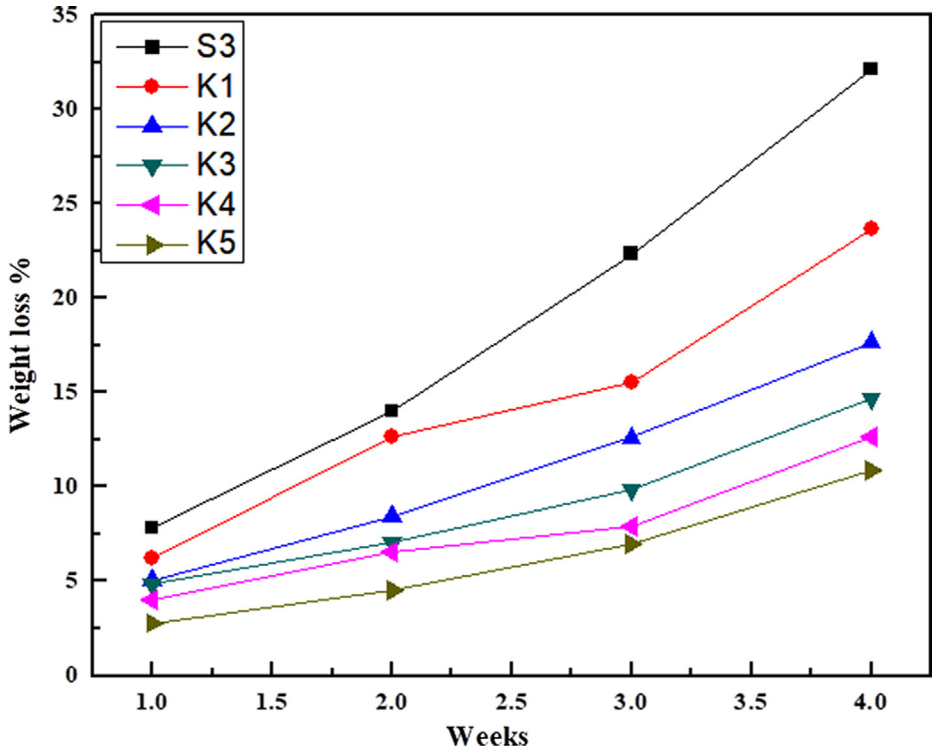

Fig. 9 Biodegradability of polymer nanocomposite films.

5.4. Differential scanning calorimetry (DSC)

DSC is a technique used to investigate thermal behavior, glass transition temperature, crystallization temperature Tc (exothermic) and melting point Tm (endothermic) of polymer nanocomposite films. The Tg of S3 composite shifts from 74 °C to 76–87 °C in polymer nanocomposite films (K1-K5) respectively. DSC results revealed that the encapsulation of NiO nanoparticles in the S3 composite increases the crosslinking/branching that obstructs the chain mobility, which leads to increases the Tg value from 74 to 87 °C as shown in Fig. 11. The significant effect on Tg temperature is due to the encapsulation of NiO nanoparticles increases the chain rigidity, molecular packing and electrostatic interaction of S3 composite (Akram et al., 2008).

DSC shows only two endothermic peaks at 193 °C and 274 °C which corresponds to the melting of polymers and there is release of strain and disintegration of C-C linkage at 426 °C resulting in the decomposition of S3 composite. The drift in the thermogram takes place from S3 composite film to three endothermic peaks at 114 °C, 119 °C and 280 °C in polymer nanocomposite (K1) films. The polymer nanocomposite (K2) film shows three endothermic peaks at 130 °C, 204 °C, 280 °C and three endothermic peaks at 132 °C, 202 °C and 281 °C shown by (K3) polymer nanocomposite film. In the nanocomposite (K4) film three endothermic peaks at 130 °C, 206 °C and 285 °C. The polymer nanocomposite (K5) also shows three endothermic peaks at 130 °C, 206 °C and 286 °C as shown in Fig. 11. The shifting of endothermic and exothermic peaks by the addition of In_2O_3 nano crystals in PVA increases the thermal stability (Singhal et al., 2012). The first endotherm peaks appeared in the polymer nanocomposites (K1-K5) is due to encapsulation of NiO nanoparticles and melting (Tm) of polymer breaks down the cross-linking and reduces the internal strain leads to decomposition of polymer nanocomposites (Osuntokun and Ajibade, 2016).

6. Adsorption studies

CR dye is one of the important textile industrial azo dye, easily soluble in water and has been deserted due to carcinogenic behaviour (Mall et al., 2005). The toxic CR dye adsorption by polymer nanocomposite films (K1-K5) were determined by three parameters such as, an effect of contact time from 15 to 200 min, an effect of the pH solution and an effect of CR dye concentration with respect to time. This present observation deals with the S3 composite film and prepared polymer nanocomposite films (K-K5) as adsorbents for the extraction of CR dye as shown in Fig. 12. The process of dye adsorption is related to equilibrium

Dye in bulk + solid adsorbed ⇄ **Dye adsorbed on surface of adsorbent**

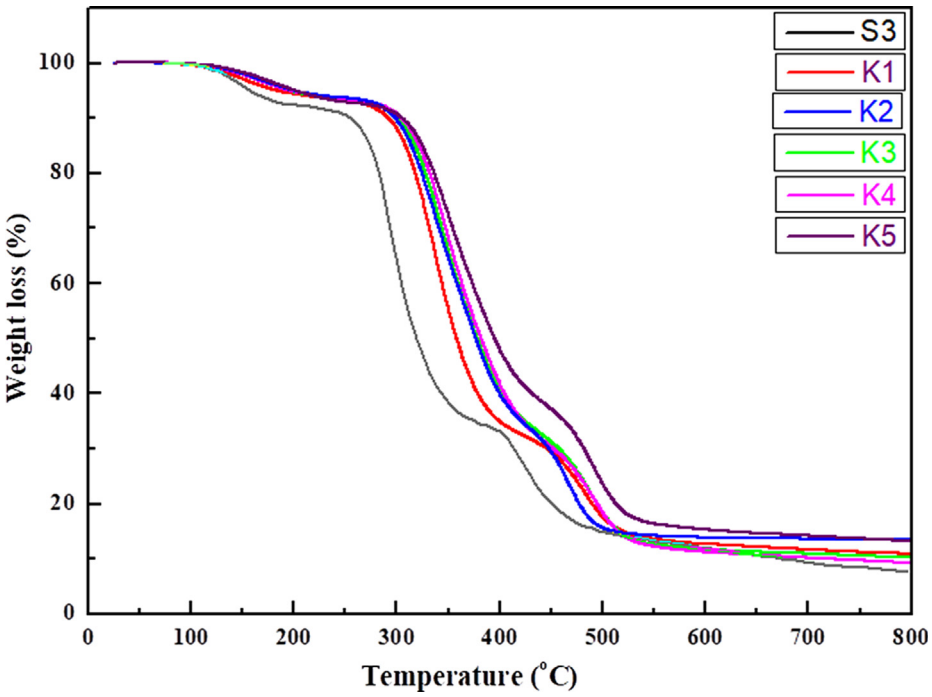

Fig. 10 TGA of S3 composite and polymer nanocomposite films.

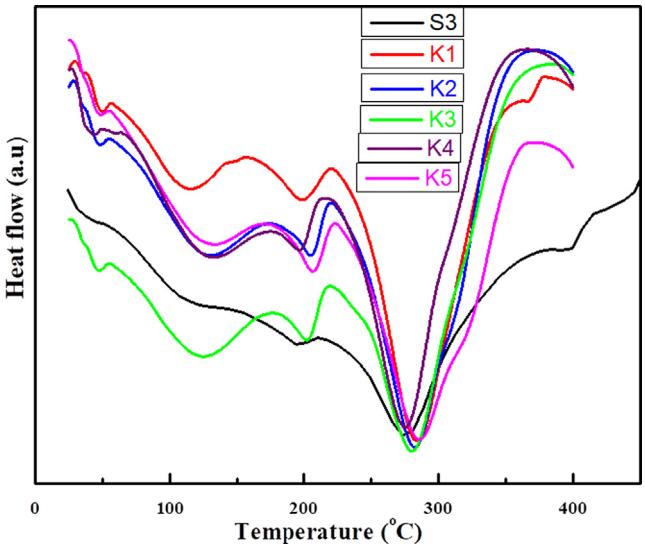

Fig. 11 DSC of (S3) composite and polymer nanocomposites films.

6.1. Effect of contact time on CR dye adsorption

The effect of the contact time on dye adsorption of CR dye is shown in Fig. 13(a).

Initially when the contact time of S3 composite to polymer nanocomposite film increases, the large surface area of NiO nanoparticles and unfilled sites are free to bind with the CR dye, which enhance the dye adsorption. The adsorption of CR dye by adsorbent beads increases as the time increases from (28–47%) in 15–100 min, then adsorption attains equilibrium in pH 7 at 37 °C (Chatterjee et al., 2007). The adsorption increases significantly from (47 to 78%) S3 to K5, due to large surface of NiO nanoparticles in the S3 composite up to certain limit then the equilibrium was attained. The result of dye adsorption can be clearly observed from the Fig. 13(a) that the S3 composite film shows minimum adsorption capacity as compared to polymer nanocomposite films (K1-K5).

6.2. Effect of pH solution on CR dye adsorption

The pH of aqueous solution plays an important role in CR dye adsorption potential of polymer nanocomposites adsorbent beads. The colour of CR dye solution changes into dark blue colour when pH attuned in high acidic range and becomes dark blue at high basic range. The adsorption of CR dye by S3 composite and nanocomposite films (K1-K5) is inversely proportional to the pH scale of the CR dye solution as shown in Fig. 13(b). The CR dye adsorption increases from S3 composite to K5 polymer nanocomposites. The adsorption of CR dye decreases in S3 composite (45–10%) and in the polymer nanocomposites (K1) 47–10% and (K5) 68–25% as the pH value increase from (4, 6,7,8,9 and 10) respectively. In the acidic media, CR dye develops more positive charged ions like NH_4^+ appears as main product followed by NO_3^- and SO_4^{2-} and the polymer nanocomposites carry OH^- and NH groups develop. The a strong electrostatic attraction between positively NH_4^+ of CR dye and negatively OH^- and NH functional groups of polymer nanocomposites in lower pH solution [66*]. The dye adsorption decrease as the pH of the solution increases because the increase of the pH leads to formation of alkaline medium that increases the negatively charged ions and reduce the numbers of positively charged ions. The electrostatic repulsion between the negatively charged CR dye and large number of negative ions in the basic medium

decrease the dye adsorption by increasing pH of the solution (Patel and Vashi, 2012). The protonation of polymer nanocomposite films decreases as the pH increases from (4, 6, 8, 9, and 10) and the CR dye adsorption decreases with increases of the pH in solution. The adsorption from S3 to K5 increases due to electrostatic interaction between the S3 composite and large surface area of nanoparticles

6.3. Effect of CR dose on the adsorption

The CR dye adsorption by S3 composite and polymer nanocomposite has been observed in 50–200 ppm concentration with respect time shown in Fig. 13(c). In order to analyze the maximum adsorption of CR dye by S3 composite and polymer nanocomposite (K1-K5) adsorbent beads. The effect of initial CR dye concentration was investigated by changing the initial dye concentration from 50 to 200 ppm at 37 °C with respect 30 min. The adsorption of dye dramatically increased as the dye concentration increases due to the presence of large number of active sites on the adsorbent (Hosseinzadeh and Khoshnood, 2016). It is clear from Fig. 13(c) that the dye adsorption of CR dye increases in the polymer nanocomposite films (K1-K5) after the encapsulation of NiO nanoparticles compared to S3 composite film. The nano size and the large surface area of NiO nanoparticles increase the CR dye adsorption in the polymer nanocomposites.

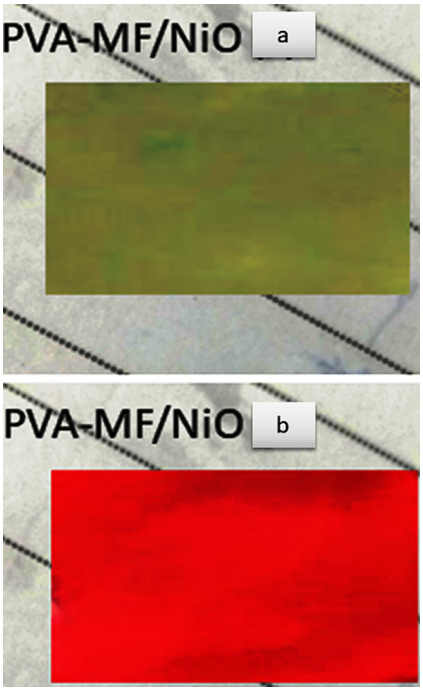

Fig. 12 Before (a) and after (b) CR dye adsorption of polymer nanocomposite film.

7. In vitro antibacterial activity

The antibacterial activity of polymer nanocomposite films (K1-K5) was investigated against Gram-positive bacterial strains *Bacillus subtilis* MTCC 736, *Staphylococcus aureus* MTCC 902 and Gram-negative *Escherichia coli* ATCC 25922 and *Klebsiella pneumoniae* ATCC 700603. The clear Zone of Inhibition (ZOI) around the polymer nanocomposite film on culture loaded MHA plates indicated antibacterial efficacy is shown in Fig. 14. The obtained Zone of Inhibition (ZOI) against Gram-positive bacteria *Bacillus subtilis* MTCC 736 (0, 0, 0, 24 and 25 mm), *Staphylococcus aureus* MTCC 902 (21, 24, 23, 25 and 25 mm) was more as compared to Gram-negative *Escherichia coli* ATCC 25922 (21, 0, 0, 22 and 22 mm) and *Klebsiella pneumoniae* ATCC 700603 (0, 0, 0, 23 and 23 mm) is shown in Table 1. The antibacterial activity against tested bacterial strains found to increases as the NiO concentration increases from 1 to 5 wt% in the polymer nanocomposites. Previous study also reported that enhancement of antibacterial activity of polypyrrole/silver nanocomposite by NiO nanoparticles against both Gram-positive and Gram-negative bacteria (Das et al., 2013; Punitha et al., 2015).

The mechanism and antibacterial efficiency of polymer nanocomposite films (K1-K5) depend on the different factors like size of NiO nanoparticles, concentration and distribution (Raghupathi et al., 2011) along with the type of interaction with S3 composite. The electrostatic interaction between NiO nanoparticles and S3 composite prevents the abrupt release

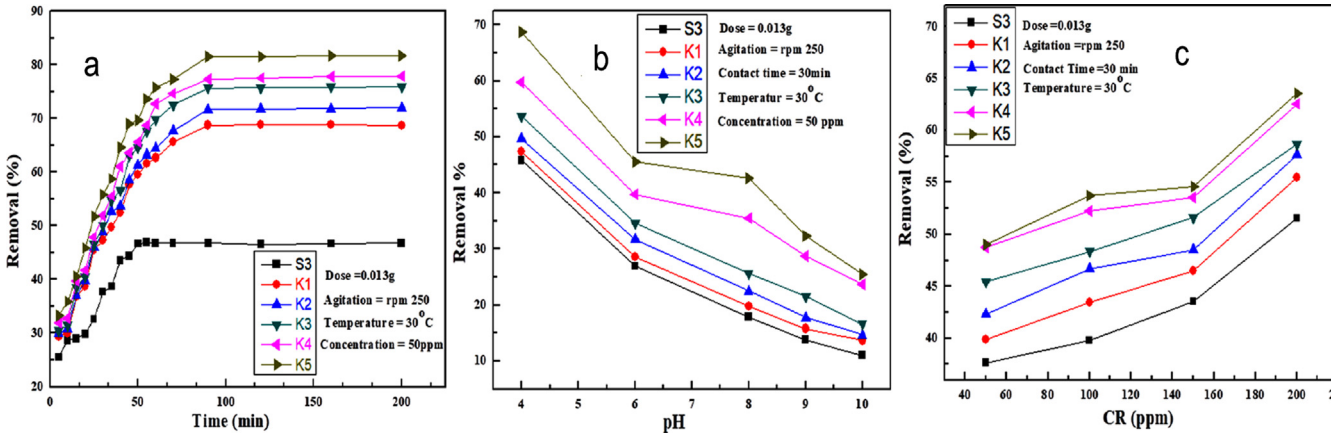

Fig. 13 (a) An effect of the contact time (b) an effect of pH solution (c) and effect of CR dye concentration on S3 composite and polymer nanocomposites for the % removal of CR dye.

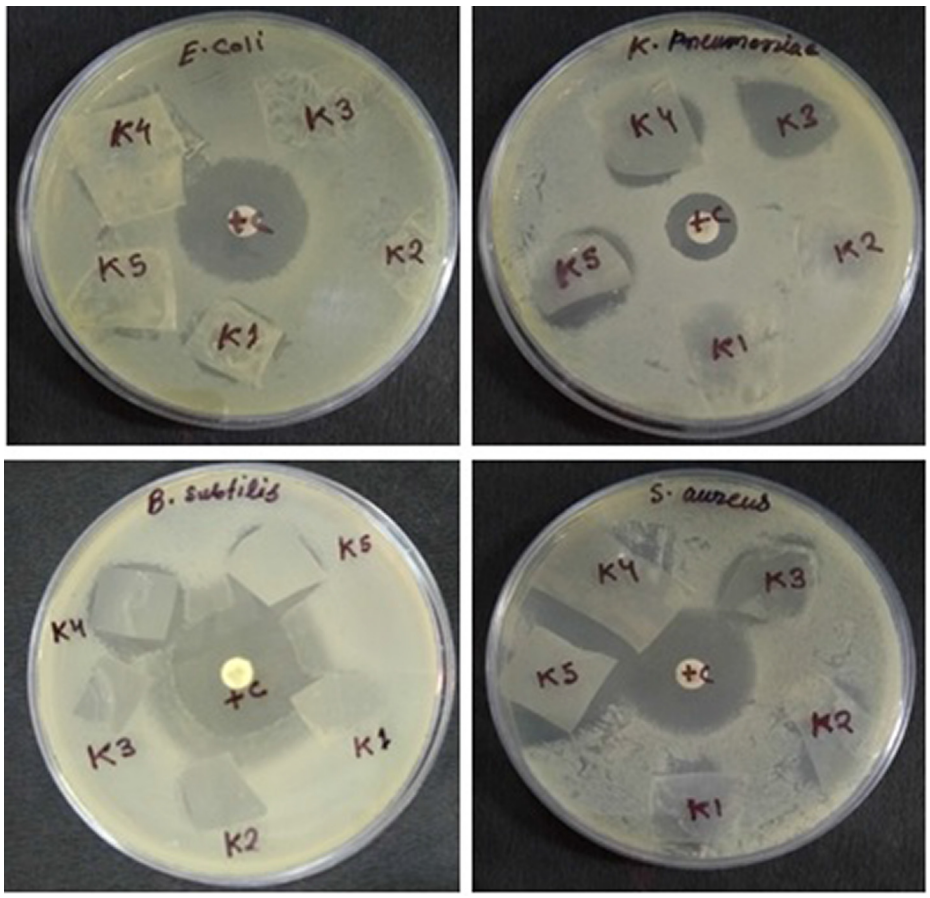

Fig. 14 Plates showing zone of inhibition (ZOI) around polymer nanocomposite films (K1-K5) against Gram-positive *Bacillus subtilis* MTCC 736, *Staphylococcus aureus* MTCC 902 and Gram-negative *Escherichia coli* ATCC 25922, *Klebsiella pneumoniae* ATCC 700603.

Table 1 Showing Zone of Inhibition (mm) for polymer nanocomposite films.

Bacterial strains	K1	K2	K3	K4	K5	+ Control
***E. coli* 25922**	21	0	0	22	22	25
***K. pneumoniae* 700603**	0	0	0	23	23	19
***Bacillus subtilis* 4736**	0	0	0	24	25	25
***Staphylococcus aureus* 5902**	21	24	23	25	25	26

of nanoparticles from the matrix, ensures long-lasting antibacterial property of polymer nanocomposites films. It is clear from the results that the bactericidal strains such as *B. subtilis* 4736 and *S. aureus* 5902 were most susceptible to polymer nanocomposites as compared to Gram negative bacteria *E. coli* 25922 and *K. pneumoniae* 70060. The Gram-negative bacterial strains possess different components in the cell wall. An outer phospholipidic membrane with largely negative charged structural lipopolysaccharide unites which restricts the entry of bioactive negatively charged polymer nanocomposites (Harada et al., 2017; Simoncic and Tomsic, 2010).

8. Conclusion

The dual functionality of polymer nanocomposite films (K1-K5) (dye adsorption and antibacterial) was developed by encapsulation of NiO nanoparticles in the S3 composite. The present work introduces an innovative, inexpensive, extensively applicable and eco-friendly method to prepare uniform smooth, free standing, hydrophobic and biodegradable polymer nanocomposite thin films. FT-IR determined the chemical bonding, molecular structure and functional groups. XRD analysis revealed that the crystallinity of S3 composite increases as the NiO nanoparticles increases. SEM observed the degree of dispersion of NiO nanoparticles in polymer nanocomposites and S3 composite surface morphology. The enhancement of thermal stability was attributed to intermolecular crosslinking and hydrogen bonding with nanoparticles. DSC thermograms of polymer nanocomposite films shown one single broad glass transition peak temperature, but the peak shifts compared to composite. The S3 composite showed maximum swelling property but least stable as compared to polymer nanocomposite films and the chemical stability enhanced from S3 to K5 in all three parameters like water,

HCl and NaOH solutions. The contact angle of polymer nanocomposite films K1-K5 (56–90°) increases with the rise of NiO nanoparticle dose, but the soil degradation decreases from S3-K5 (32–7%). The percent removal of CR dye adsorption of CR increased from S3 to K5 due to small size of NiO nanoparticles encapsulated in the S3 composite. The polymer nanocomposites showed antibacterial activity against *E. coli* 25922 25 mm, *K. pneumoniae* 700603 23 mm, *B. subtilis* 4736 25 mm and *S. aureus* 5902 25 mm based on the data presented in the manuscript**.** This study not only displays a promising strategy for fabricating of versatile polymer nanocomposites but also contributes to the understanding and the design of polymer nanocomposites with desired properties such as adsorption of toxic CR dye and antibacterial activity.

Acknowledgements

Author S. A. Bhat wishes to acknowledge University Grants Commission, New Delhi, India for non-Net Fellowship. Dr. F. Zafar is thankful to Dept. of science & Technology, New Delhi, India for the fellowship of Women Scientists Scheme (WOS) for research in basic/applied Science (Ref.no.-SR/WOSA/CS-97/2016). Authors thanks to Centre Instrumentation Facilities, Centre for Interdisciplinary Research in Basic Science, Jamia Millia Islamia for FTIR, XRD and UV. Authors are also thankful to the Head, Dept. of Chemistry, Jamia Millia Islamia, for providing facilities to carry out the research work.

References

Ahad, N., Saion, E., Gharibshahi, E., 2012. Structural, thermal, and electrical properties of Pva-sodium salicylate solid composite polymer electrolyte. J. Nanomater. 6 (5), 2012.

Ahmad, R., Kumar, R., 2010. Adsorptive removal of CR dye from aqueous solution using bael shell carbon. Appl. Surf. Sci. 257 (5), 1628–1633.

Ahmad, M., Manzoor, K., Chaudhuri, R.R., Ikram, S., 2017. Thiocarbohydrazide cross-linked oxidized chitosan and poly(vinyl alcohol): a green framework as efficient Cu(II), Pb(II), and Hg(II) adsorbent. J. Chem. Eng. Data. 62 (7), 2044–2055.

Ajoudanian, N., Nezamzadeh-Ejhieh, A., 2015. Enhanced photocatalytic activity of nickel oxide supported on clinoptilolite nanoparticles for the photodegradation of aqueous cephalexin. Mater. Sci. Semicond. Process. 36, 162–169.

Akram, D., Sharmin, E., Ahmad, S., 2008. Synthesis, characterization and corrosion protective properties of boron-modified polyurethane from natural polyol. Prog. Org. Coatings. 277, 130–137.

Anisha, B.S., Biswas, R., Chennazhi, K.P., Jayakumar, R., 2013. Chitosan-hyaluronic acid/nano silver composite sponges for drug resistant bacteria infected diabetic wounds. Int. J. Biol. Macromol. 62, 310–320.

Ayad, M.M., El-Nasr, A.A., 2010. Adsorption of cationic dye (methylene blue) from water using polyaniline nanotubes base. J. Phys. Chem. C. 66, 1–35.

Ayeshamariam, A., Sankaracharyulu, G.V., Kashif, M., Hussain, S., Bououdina, M., Jayachandran, M., 2015. Antibacterial activity studies of Ni and SnO < inf > 2 < /Inf > loaded chitosan beads. Mater. Sci. form. 832, 110–122.

Azizi, S., Ahmad, M.B., Ibrahim, N.A., Hussein, M.Z., Namvar, F., 2014. Cellulose nanocrystals/ZnO as a bifunctional reinforcing nanocomposite for poly(vinyl alcohol)/chitosan composite films: fabrication, characterization and properties. Int. J. Mol. Sci. 15 (6), 11040–11053.

Bauer, A.W., Kirby, W.M., Sherris, J.C., Turck, M., 1966. Antibiotic susceptibility testing by a standardized single disk method. Am. J. Clin. Pathol. 45 (4), 493–496.

Bhargav, P.B., Mohan, V.M., Sharma, A.K., Rao, V.V.R.N., 2009. Investigations on electrical properties of (PVA:NaF) polymer electrolytes for electrochemical cell applications. Curr. Appl. Phys. 9 (1), 165–171.

Bhat, S.A., Kareem, A., Mohammad, A., Zafar, F., Nishat, N., 2019. Development and electrical conductivity of PVA/MF-based nanocomposite doped with NiO nanoparticles. Ionics (Kiel). 25 (5), 2183–2193.

Bhat, S.A., Zafar, F., Mondal, A.H., Kareem, A., Mirza, A.U., Khan, S., Mohammad, A., Haq, Q.M.R., Nishat, N., 2019. Photocatalytic degradation of carcinogenic Congo red dye in aqueous solution, antioxidant activity and bactericidal effect of NiO nanoparticles. J. Iran. Chem. Soc. https://doi.org/10.1007/s13738-019-01767-3.

Bhat, S.A., Zafar, F., Mondal, A.H., Mirza, A.U., Mohammad, A., Haq, Q.M.R., Nishat, N., 2020. Efficient removal of congo red dye from aqueous solution by adsorbent films of polyvinyl alcohol/melamine-formaldehyde composite and bactericidal effects. J. Cleaner Prod. 255 (10). 120062.

Chatterjee, S., Chatterjee, S., Chatterjee, B.P., Guha, A.K., 2007. Adsorptive removal of CR, a carcinogenic textile dye by chitosan hydrobeads: binding mechanism, equilibrium and kinetics. Colloids Surf. A Physicochem. Eng. Asp. 299 (1–3), 146–152.

Choma, J., Jedynak, K., Marszewski, M., Jaroniec, M., 2012. Polymer-templated mesoporous carbons synthesized in the presence of nickel nanoparticles, nickel oxide nanoparticles, and nickel nitrate. Appl. Surf. Sci. 258 (8), 3763–3770.

Das, D., Nath, B.C., Phukon, P., Saikia, B.J., Kamrupi, I.R., Dolui, S. K., 2013. Nickel oxide/polypyrrole/silver nanocomposites with core/shell/shell structure: synthesis, characterization and their electrochemical behaviour with antimicrobial activities. Mater. Chem. Phys. 142 (1), 61–69.

DeMerlis, C.C., Schoneker, D.R., 2003. Review of the oral toxicity of PVA (PVA). Food and Chem. Toxi. 41 (3), 319–326.

Elbarbary, A.M., El-Sawy, N.M., 2017. Radiation synthesis and characterization of PVA/chitosan/silver nanocomposite membranes: antimicrobial and blood compatibility studies. Polym. Bull. 74 (1), 195–212.

Elbarbary, A.M., El-Sawy, N.M., 2017. Radiation synthesis and characterization of polyvinyl alcohol/chitosan/silver nanocomposite membranes: antimicrobial and blood compatibility studies. Polym. Bull. 74 (1), 195–212.

El-Kemary, M., Nagy, N., El-Mehasseb, I., 2013. Nickel oxide nanoparticles: synthesis and spectral studies of interactions with glucose. Mater. Sci. Semicond. Process. 16 (6), 1747–1752.

Farzaneh, F., Haghshenas, S., 2012. Facile synthesis and characterization of nanoporous NiO with folic acid as photodegredation catalyst for CR. Mater. Sci. Appl. 3, 697–703.

Gandhi, S., Nagalakshmi, N., Baskaran, I., Dhanalakshmi, V., Nair, M.R.G., Anbarasan, R., 2010. Synthesis and characterization of nano-sized NiO and its surface catalytic effect on poly(vinyl alcohol). J. Appl. Polym. Sci. 118 (8), 1667–1672.

Gerlach, G., Guenther, M., Sorber, J., Suchaneck, G., Arndt, K.F., Richter, A., 2005. Chemical and PH sensors based on the swelling behavior of hydrogels. Sens. Actuators, B 111 (2), 555–561.

Gopishetty, V., Tokarev, I., Minko, S., 2012. Biocompatible stimuli-responsive hydrogel porous membranes via phase separation of a PVA and Na-alginate intermolecular complex. J. Mater. Chem. 22 (37), 19482–19487.

Guo, Q., Ghadiri, R., Weigel, T., Aumann, A., Gurevich, E.L., Esen, C., Medenbach, O., Cheng, W., Chichkov, B., Ostendorf, A., 2014. Comparison of in Situ and ex situ methods for synthesis of two-photon polymerization polymer nanocomposites. Polymers (Basel) 6 (7), 2037–2050.

Guzman-Puyol, S., Ceseracciu, L., Heredia-Guerrero, J.A., Anyfantis, G.C., Cingolani, R., Athanassiou, A., Bayer, I.S., 2015. Effect of

trifluoroacetic acid on the properties of PVA and PVA-cellulose composites. Chem. Eng. J. 277, 242–251.
Harada, T., Mizuno, M., Kato, T., 2017. Studies on the antibacterial activity of fungi. I. Yakugaku zasshi 72 (4), 591–593.
Hassiba, A.J., El Zowalaty, M.E., Webster, T.J., Abdullah, A.M., Nasrallah, G.K., Khalil, K.A., Luyt, A.S., Elzatahry, A.A., 2017. Synthesis, characterization, and antimicrobial properties of novel double layer nanocomposite electrospun fibers for wound dressing applications. Int. J. Nanomedicine. 12, 2205–2213.
Helan, V., Prince, J.J., Al-Dhabi, N.A., Arasu, M.V., Ayeshamariam, A., Madhumitha, G., Roopan, S.M., Jayachandran, M., 2016. Neem leaves mediated preparation of NiO nanoparticles and its magnetization, coercivity and antibacterial analysis. Res. Phys. 6, 712–718.
Hosseinzadeh, H., Khoshnood, N., 2016. Removal of cationic dyes by poly(AA-Co-AMPS)/montmorillonite nanocomposite hydrogel. Desalin. Water Treat. 57 (14), 22–43.
Hsieh, H.-T., Chang, H.-M., Lin, W.-J., Hsu, Y.-T., Mai, F.-D., 2017. Poly-methyl methacrylate/PVA copolymer agents applied on diabetic wound dressing. Sci. Rep. 7 (1), 9531.
Hu, D., Wang, L., 2016. Preparation and characterization of antibacterial films based on PVA/quaternized cellulose. React. Funct. Polym. 101, 90–98.
Ichiyanagi, Y., Wakabayashi, N., Yamazaki, J., Yamada, S., Kimishima, Y., Komatsu, E., Tajima, H., 2003. Magnetic properties of NiO nanoparticles. Physica B 329–333, 862–863.
Issa, A.T., Schimmel, K.A., Worku, M., Shahbazi, A., Ibrahim, S.A., Tahergorabi, R., 2018. Sweet potato starch-based nanocomposites: development, characterization, and biodegradability. Starch/Staerke 74 (8), 1700273.
Joo, J.B., Park, J., Yi, J., 2009. Preparation of polyelectrolyte-functionalized mesoporous silicas for the selective adsorption of anionic dye in an aqueous solution. J. Hazard. Mater. 168 (1), 102–107.
Kandelbauer, A., Wuzella, G., Mahendran, A., Taudes, I., Widsten, P., 2009. Using isoconversional kinetic analysis of liquid melamine-formaldehyde resin curing to predict laminate surface properties. J. Appl. Polym. Sci. 113 (4), 2649–2660.
Karthik, K., Selvan, G.K., Kanagaraj, M., Arumugam, S., Jaya, N.V., 2011. Particle size effect on the magnetic properties of NiO nanoparticles prepared by a precipitation method. J. Alloys Compd. 509 (1), 181–184.
Kashihara, K., Uto, Y., Nakajima, T., 2018. Rapid in situ synthesis of polymer-metal nanocomposite films in several seconds using a CO2laser. Sci. Rep. 8 (1), 14719–14728.
Lakouraj, M.M., Norouzian, R.S., Balo, S., 2015. Preparation and cationic dye adsorption of novel Fe < inf > 3 < /Inf > O < inf > 4 < /Inf > supermagnetic/thiacalix[4]arene tetrasulfonate self-doped/polyaniline nanocomposite: kinetics, isotherms, and thermodynamic study. J. Chem. Eng. Data. 60 (8), 2262–2272.
Likozar, B., Koroec, R.C., Poljanek, I., Ogorelec, P., Bukovec, P., 2012. Curing kinetics study of melamine-urea-formaldehyde resin. J. Ther. Analys. Calor. 109, 1413–1422.
Longo, A., Carotenuto, G., Palomba, M., De Nicola, S., 2011. Dependence of optical and microstructure properties of thiol-capped silver nanoparticles embedded in polymeric matrix. Polymers (Basel). https://doi.org/10.3390/polym3041794.
Mahdavinia, G.R., Massoudi, A., Baghban, A., Shokri, E., 2014. Study of adsorption of cationic dye on magnetic kappa-carrageenan/PVA nanocomposite hydrogels. J. Environ. Chem. Eng. 2 (3), 1578–1587.
Mall, I.D., Srivastava, V.C., Agarwal, N.K., Mishra, I.M., 2005. Removal of congo red from aqueous solution by bagasse fly ash and activated carbon: kinetic study and equilibrium isotherm analyses. Chemosphere 61 (1), 492–501.
Mandelbaum, R.T., Allan, D.L., Wackett, L.P., 1995. Isolation and characterization of a Pseudomonas Sp. that mineralizes the s-triazine herbicide atrazine. Appl. Environ. Microbiol. 61, 1451–1457.
Matsuda, S.I., Yasuda, Y., Ando, S., 2005. Fabrication of polyimide-composite thin films containing uniformly oriented silver nanorods and their use as flexible, linear polarizers. Adv. Mater. 17 (33), 2221–2224.
Meftah, A.M., Gharibshahi, E., Soltani, N., Mat Yunus, W.M., Saion, E., 2014. Structural, optical and electrical properties of PVA/PANI/Nickel nanocomposites synthesized by gamma radiolytic method. Polymers (Basel) 6 (9), 2435–2450.
Mendoza Zélis, P., Muraca, D., Gonzalez, J.S., Pasquevich, G.A., Alvarez, V.A., Pirota, K.R., Sánchez, F.H., 2013. Magnetic properties study of iron-oxide nanoparticles/PVA ferrogels with potential biomedical applications. J. Nanoparticle Res. 15 (5), 1613.
Merline, D.J., Vukusic, S., Abdala, A.A., 2013. Melamine formaldehyde: curing studies and reaction mechanism. Polym. J. 45 (4), 413–419.
Osuntokun, J., Ajibade, P.A., 2016. Structural and thermal studies of ZnS and CdS nanoparticles in polymer matrices. J. Nanomater. 23 (3), 23–55.
Pal, S., Ghorai, S., Das, C., Samrat, S., Ghosh, A., Panda, A.B., 2012. Carboxymethyl tamarind-g-poly(acrylamide)/silica: a high performance hybrid nanocomposite for adsorption of methylene blue dye. Ind. Eng. Chem. Res. 51 (48), 15546–15556.
Patel, H., Vashi, R.T., 2012. Removal of CR dye from its aqueous solution using natural coagulants. J. Saudi Chem. Soc. 16 (2), 44–65.
Pirzada, T., Arvidson, S.A., Saquing, C.D., Shah, S.S., Khan, S.A., 2012. Hybrid silica-PVA nanofibers via sol-gel electrospinning. Langmuir 28 (13), 5834–5844.
Pourjavadi, A., Abedin-Moghanaki, A., Tavakoli, A., 2016. Efficient removal of cationic dyes using a new magnetic nanocomposite based on starch-g-poly(vinylalcohol) and functionalized with sulfate groups. RSC Adv. 6 (44), 38042–38051.
Punitha, N., Ramesh, P.S., Spectral, Geetha D., 2015. Morphological and antibacterial studies of β-cyclodextrin stabilized silver - chitosan nanocomposites. Spectrochim. Acta - Part A Mol. Biomol. Spectrosc. 5 (136), 1710–1717.
Raghupathi, K.R., Koodali, R.T., Manna, A.C., 2011. Size-dependent bacterial growth inhibition and mechanism of antibacterial activity of zinc oxide nanoparticles. Langmuir 27 (7), 4020–4028.
Razavi, S., Sabetghadam, A., Mohammadi, T., 2011. Dehydration of isopropanol by PVA-APTEOS/TEOS nanocomposite membranes. Chem. Eng. Res. Des. 89 (2), 148–155.
Rudko, G.Y., Kovalchuk, A.O., Fediv, V.I., Ren, Q., Chen, W.M., Buyanova, I.A., Pozina, G., 2013. Role of the host polymer matrix in light emission processes in nano-CdS/poly vinyl alcohol composite. Thin Solid Films 543, 11–15.
Satheesh Kumar, M.N., 2007. Studies on melamine formaldehyde (MF) loaded polyvinyl acetate-polyester nonwoven fabric composites. J. Thermoplast. Compos. Mater. 20 (3), 305–322.
Sekhavat Pour, Z., Ghaemy, M., 2015. Removal of dyes and heavy metal ions from water by magnetic hydrogel beads based on poly (vinyl alcohol)/carboxymethyl starch-g-poly(vinyl imidazole). RSC Adv. 22, 19482.
Simoncic, B., Tomsic, B., 2010. Structures of novel antimicrobial agents for textiles - a review. Text. Res. J. 80 (16), 1721–1737.
Singhal, A., Kaur, M., Dubey, K.A., Bhardwaj, Y.K., Jain, D., Pillai, C.G.S., Tyagi, A.K., 2012. PVA-In < inf > 2 < /Inf > O < inf > 3 < /Inf > nanocomposite films: synthesis, characterization and gas sensing properties. RSC Adv. 5 (38), 30297–30302.
Thakur, S., Pandey, S., Arotiba, O.A., 2016. Development of a sodium alginate-based organic/inorganic superabsorbent composite hydrogel for adsorption of methylene blue. Carbohydr. Polym. 153, 34–46.
Udagawa, A., Fujie, T., Kawamoto, Y., Saito, A., Takeoka, S., Asahi, T., 2016. Interfacial effects on the crystallization and surface properties of poly(l-lactic acid) ultrathin films. Polym. J. 48 (2), 157–161.

Vaghela, S.S., Jethva, A.D., Mehta, B.B., Dave, S.P., Adimurthy, S., Ramachandraiah, G., 2005. Laboratory studies of electrochemical treatment of industrial azo dye effluent. Environ. Sci. Technol. 39 (8), 2848–2855.

Wang, Q., 2015. Robust and thermal-enhanced melamine formaldehyde-modified glassfiber composite separator for high-performance lithium batteries. Electrochim. Acta 182, 334–341.

Wei, K., Liu, N., Li, L., Zheng, S., 2015. A stereoregular macrocyclic oligomeric silsesquioxane bearing epoxide groups: synthesis and its nanocomposites with polybenzoxazine. RSC Adv. 6–43, 77274–77287.

Wu, Y., Liu, J., Ma, J., Liu, Y., Wang, Y., Wu, D., 2016. Ratiometric nanothermometer based on rhodamine dye-incorporated f127-melamine-formaldehyde polymer nanoparticle: preparation, characterization, wide-range temperature sensing, and precise intracellular thermometry. ACS Appl. Mater. Interfaces. 8 (23), 14396–14405.

Xu, W., Dong, S., Yu, C., Yan, X., Xu, J., Jiang, M., 2014. Melamine formaldehyde/PVA composite fiber: structure and properties manipulated by hydroxymethylation degree. J. Appl. Polym. Sci. 131 (17), 8491–8497.

Yang, Y., Wei, Z., Wang, C., Tong, Z., 2013. Versatile fabrication of nanocomposite microcapsules with controlled shell thickness and low permeability. ACS Appl. Mater. Interfaces 5 (7), 2495–2502.

Yu, C., Xu, W., Zhao, X., Xu, J., Jiang, M., 2014. Effects of the reaction degree of melamine-formaldehyde resin on the structures and properties of melamine-formaldehyde/PVA composite fiber. Fibers Polym. 15 (9), 1828–1834.

Zhou, J., Lü, Q.F., Luo, J.J., 2018. Efficient removal of organic dyes from aqueous solution by rapid adsorption onto polypyrrole-based composites. J. Clean. Prod. 167, 739–748.